HHS Public Access

Author manuscript

J Invest Dermatol. Author manuscript; available in PMC 2024 October 01.

Published in final edited form as:

J Invest Dermatol. 2023 October ; 143(10): 2052–2064.e5. doi:10.1016/j.jid.2023.03.1671.

Bacterial Pyocyanin Inducible KRT6A Accelerates Closure of Epithelial Defect Under Conditions of Mitochondrial Dysfunction

Subhadip Ghatak[1], **Craig Hemann**[2], **James Boslett**[2,3], **Kanhaiya Singh**[1], **Anu Sharma**[1], **Mohamed S. El Masry**[1], **Ahmed Safwat Abouhashem**[1], **Nandini Ghosh**[1], **Shomita S Mathew-Steiner**[1], **Sashwati Roy**[1], **Jay L. Zweier**[2], **Chandan K. Sen**[1,*]

[1]Indiana Center for Regenerative Medicine and Engineering, Department of Surgery, Indiana University School of Medicine, Indianapolis, IN- 46202, USA

[2]Department of Internal Medicine, Division of Cardiovascular Medicine, Davis Heart & Lung Research Institute, College of Medicine, The Ohio State University, Columbus, OH 43210, USA

[3]Department of Cell Biology, University of Pittsburgh School of Medicine, Pittsburgh, Pennsylvania, USA (current institution)

Abstract

Repair of epithelial defect is complicated by infection and related metabolites. Pyocyanin is one such metabolite which is secreted during *Pseudomonas aeruginosa* infection. Keratinocyte migration is required for the closure of skin epithelial defects. The current work sought to understand pyocyanin-keratinocyte interaction and its significance in tissue repair. SILAC proteomics identified mitochondrial dysfunction as the top pathway responsive to pyocyanin exposure in human keratinocytes. Consistently, functional studies demonstrated mitochondrial stress, depletion of reducing equivalents, and ATP. Strikingly, despite all the above, pyocyanin markedly accelerated keratinocyte migration. Investigation of underlying mechanisms revealed a new function of KRT6A in keratinocytes. KRT6A was pyocyanin inducible and accelerated closure of epithelial defect. Acceleration of closure was associated with poor quality healing including compromised expression of apical junction proteins. This work recognizes KRT6A for its role of enhancing keratinocyte migration under conditions of threat posed by pyocyanin. Qualitatively deficient junctional proteins under conditions of defensive acceleration of keratinocyte migration explains why an infected wound close with deficient skin barrier function as previously reported.

[*]To whom correspondence should be addressed: Chandan K. Sen, Ph.D, Indiana Center for Regenerative Medicine and Engineering (ICRME), Department of Surgery, Indiana University School of Medicine, Indianapolis, IN-46202. cksen@iu.edu; Tel: + 317-278-2736; Twitter: @ChandanKSen.

AUTHOR CONTRIBUTIONS

Conceptualization: C.K.S; Methodology: S.G, C.H J.B, A.S, and J.L.Z; Data Analysis:, S.G, A.S, M.E.M, A.S.A, N.G, S.S.M.S, C.H, J.B and K.S; Writing – Strategy & Original Draft: S.G, S.R, and C.K.S; Review & Editing: C.K.S, S.R, J.L.Z, C.H, J.B, K.S; Funding Acquisition: C.K.S.

CONFLICT OF INTERESTS

The authors declare no competing interest.

Keywords

Pseudomonas aeruginosa ; Pyocyanin; Reactive Oxygen Species; Mitochondria; KRT6A; Migration; Junctional Proteins

INTRODUCTION

Repair of epithelial injury is complicated by infection (Ruffin and Brochiero, 2019). *Pseudomonas aeruginosa* is commonly involved in such infections (Mihai et al., 2014). Skin is the largest organ of the human body, responsible for barrier function safeguarding the internal environment of the body from external threats such as allergens and pathogens. *P. aeruginosa* is opportunistic, exploiting breaches in host defenses to initiate and establish infections. During the process of establishing infection, *P. aeruginosa* produces secretory pathogenic factors including metabolites such as pyocyanin (Deng et al., 2020, Flemming and Wingender, 2010, Mittal et al., 2009). Pyocyanin forms a redox-active tricyclic zwitterion with a half-life of 8.9 hour (Van der Berg et al., 2015). Pyocyanin, detected abundantly at concentration exceeding 0.1 mM in human body fluid bathing the infected tissue (Cruickshank and Lowbury, 1953, Muller, 2006, Reimer et al., 2000, Wilson et al., 1988), is responsible for the yellowish green color and malodorous smell which are characteristics of *P. aeruginosa* infection (Norbury et al., 2016). Of particular interest is the observation that pyocyanin induces cellular and molecular responses both within the bacteria of origin as well as on host pathology (Hall et al., 2016, Mahajan-Miklos et al., 1999).

Closing an epithelial defect following injury is an evolutionarily conserved survival response. Proliferating keratinocytes feed the migrating epithelial tongue which advance to achieve closure (Woodley, 1996). The functional quality of such closure, as determined by junctional proteins responsible for cell-cell and cell-matrix contact, is of paramount significance (Golovkine et al., 2016, Ruffin and Brochiero, 2019). Poor quality closure is known to compromise barrier function of the tissue making it vulnerable to complications such as poor skin tensile strength (Roy et al., 2020). In the current work, we sought to study pyocyanin-dependent impairment of the closure of epithelial defect. This work revealed an unexpected, accelerated closure of epithelial defect *via* a KRT6A-dependent mechanism. Thus, attention was turned towards understanding the role of pyocyanin on keratinocyte pathology and KRT6A-dependent mechanisms of acute host defense.

RESULTS

Pyocyanin-sensitive proteins in human keratinocytes

Human keratinocytes were grown in light ($^{12}C_6$, $^{14}N_4$ L-Arginine + $^{12}C_6$, $^{14}N_2$ L-lysine) and heavy media ($^{13}C_6$, $^{15}N_4$ L-Arginine + $^{13}C_6$, $^{15}N_2$ L-Lysine) for six passages until there was 100% incorporation of heavy isotope in the heavy labeled cells (Figure 1a). Incorporation rate of heavy isotopes was validated by analyzing the ratio of heavy to light labeled peptides (Supplementary Figure S1a). As an example, the peak in the dotted blue box of MS1 spectrum represents high intensity of heavy labeled peptide. Keratin type II cytoskeletal 6A (ISIGGGSC$_{(CAM)}$AISGGYGSR$_{(6C134\ N15)}$; *m/*

z=804.8873) was detected wholly in its labeled heavy peptide form (MS2 spectrum). Its unlabeled light form (ISIGGGSC$_{(CAM)}$AISGGYGSR; *m/z*=799.8832) was not detected. Thus, 100% labeling was evident (Supplementary Figure S1c). Mass spectrometry of pyocyanin-exposed keratinocyte identified a total of 1,681 labeled candidate proteins (Supplemental File 1). Of these proteins, 133 (74 upregulated, 59 downregulated) were detected to be statistically significant in all replicates ($p < 0.05$, minimum 50% change in heavy/ light ratio; Figure 1b, Supplemental File 2). Based on data mining strategy illustrated in Figure 1b, most of the significantly altered proteins expressed within the ± 1 range of log ratios (Figure 1c). Ingenuity pathway analysis (IPA) of these differentially expressed proteins revealed twelve canonical pathways (–log p-value ˃ 3; Figure 1d). Mitochondrial dysfunction was detected to be the dominant candidate pathway. Of the 171 known mitochondrial dysfunction proteins in the IPA database (QIAGEN Inc., https://www.qiagenbioinformatics.com/products/ingenuitypathway-analysis), pyocyanin exposure upregulated 15 proteins. Another dominant pathway activated after pyocyanin exposure was oxidative phosphorylation, consistent with mitochondrial pathway alterations (Figure 1d). In addition, another independent gene ontology (GO) analysis using Cytoscape identified that the dominant up-regulated proteins (Figure 1e) and their pathways were associated with cell metabolism and mitochondrial respiration functional clusters (Figure 1f). Pathways related to downregulated proteins (Supplementary Figure S1b) were associated with clusters representing DNA replication, inflammatory responsive elements, amino acid synthesis and NADPH generation *via* the pentose-phosphate shunt pathway (Supplementary Figure S1c).

Pyocyanin induced mitochondrial stress

Unbiased quantitative proteomic screening of the human keratinocyte exposed to pyocyanin identified mitochondrial function as the top cellular target of pyocyanin. Follow up studies were therefore planned to test mitochondrial function in response to pyocyanin exposure (Figure 2a). Although there was no significant change in the basal oxygen consumption rate (OCR), maximal respiration was blunted in response to pyocyanin exposure (Figure 2b, Supplementary Figure S2a). Non-mitochondrial respiration was significantly increased in response to pyocyanin (Figure 2c). Extracellular acidification rate (ECAR) showed significant increase in glycolysis and glycolytic capacity in pyocyanin exposed human keratinocytes with significant drop in non-glycolytic acidification (Figure 2d, Supplementary Figure S2a). Consistently, there was increase in proton leak with significant decline in cellular ATP production rate following pyocyanin exposure (Figure 2e). Depletion of ATP was associated with elevated ADP (Supplementary Figure S2b,c). Pyocyanin-exposed keratinocytes demonstrated sharply (3.5x) lower ATP/ ADP ratio (Figure 2f). Although glycolysis was predominant in pyocyanin exposed keratinocytes, lactate accumulation was not evident (Supplementary Figure S2d).

Mitochondrial proton leak impairs coupling efficiency (Jastroch et al., 2010). Pyocyanin exposed human keratinocytes caused mitochondrial depolarization (Figure 2g, Supplementary Figure S2e). The ratio of JC-1 aggregate/monomer declined in pyocyanin-exposed cells (Figure 2h). These keratinocytes with depolarized mitochondria demonstrated significantly higher abundance of DRP1 (Figure 2i,j). Consistently, OPA1 declined (Figure 2i,j) indicating mitochondrial fragmentation. Mitochondrial network analysis showed significant decrease in mitochondrial network and branch length in pyocyanin exposed keratinocytes (Figure 2k-m).

Cellular reducing equivalents, NADH and NADPH (Supplementary Figure S2f,g), were both depleted in pyocyanin-exposed keratinocytes. While NAD, the oxidized form of NADH, was also depleted (Supplementary Figure S2f,g) NADP remain unchanged (Supplementary Figure S2f,g). Because of proportionate depletion of both NAD as well as NADH, in response to pyocyanin, cellular NADH/NAD$^+$ ratio remain unchanged (Supplementary Figure S2h). In contrast, NADPH/NADP$^+$ halved (Figure 2o,p).

Pyocyanin induced mitochondrial $O_2^{-\cdot}$ generation

Mitochondrial dysfunction is known to be associated with increased levels of superoxide anion radical. Pyocyanin-exposed keratinocytes demonstrated sharply (>2x) higher levels of mitochondrial $O_2^{-\cdot}$. Specificity of the mitochondrial signal was verified by its quenching by MnTBAP, an SOD mimetic (Figure 3a-d). Mitochondrial superoxide anion radical is detoxified by mitochondrial SOD2 or MnSOD. Pyocyanin-exposed keratinocytes demonstrated downregulated SOD2 abundance (Figure 2e,f).

H_2O_2 was measured in human keratinocytes using highly selective genetically encoded fluorescent indicator, pHyPer-cyto (Figure 3g,h). This probe, pHyPer-cyto, measures submicromolar concentrations of H_2O_2 and is insensitive to other oxidants like superoxide and nitric oxide (Belousov et al., 2006). In keratinocytes exposed to pyocyanin (10 μM, 5d), cellular H_2O_2 levels were 2-fold higher (Figure 3b). Quenching of HyPer signal on addition of catalase verified the reported specificity of the probe (Belousov et al., 2006).

Direct assessment of superoxide and secondary radical generation was conducted using electron paramagnetic resonance spectrometry (EPR) spin trapping (Figure 3i-k). As illustrated in Figure 3j, neither pyocyanin nor human keratinocytes alone were responsible for the EPR signal noted in cells exposed to pyocyanin. In such exposed cells, in the presence of the spin trap DMPO, a prominent signal of the DMPO-OH adduct was seen (Figure 3j,k). The DMPO-OH signal appeared as a 1:2:2:1 quartet with hyperfine splitting aH = aN = 14.9 G. Quantification of peak intensities indicated the generation of approximately 170 nM DMPO-OH adduct in the pyocyanin-exposed cells. With the objective to determine the observed signal, superoxide dismutase (SOD1) and catalase (CAT) were added separately to pyocyanin-exposed keratinocytes and spectra were recorded. Addition of SOD1 almost completely quenched the DMPO-OH signal, while CAT did not have any significant quenching effect. These observations demonstrated that $O_2^{-\cdot}$ was the primary source of the observed DMPO-OH adduct.

In human keratinocytes, pyocyanin induced mitochondrial O2$^{-\cdot}$ generation and membrane depolarization was associated with sharp lowering of mitochondrial GSH (Figure 3l). HPLC chromatograms displayed lower cellular GSH (Supplementary Figure S3a-c) and unchanged GSSG (Supplementary Figure S3c) in pyocyanin-exposed keratinocytes. Thus, cellular GSH/GSSG ratio was lower in response to pyocyanin (Figure 3m).

Keratinocyte migration augmented by pyocyanin

Contrary to our original hypothesis, cell migration was accelerated in keratinocytes exposed to pyocyanin (Figure 4a-d). Within 16h, leading edges of the migration front met to close the gap. During the same time interval, native cells were only able to cover 40% of the gap. Interestingly, such faster migration was associated with hyperproliferation of pyocyanin treated keratinocytes (Supplementary Figure S4a,b). Pyocyanin-accelerated migration of keratinocytes was sensitive to both catalase as well as SOD1 indicating the participation of ROS (Figure 4a-d). At the migration front, the following set of apical junctional proteins were studied: ZO-1, ZO-2, claudin 1, claudin 4, occludin, JAM-A, tricellulin, E-cadherin and β-catenin (Figure 4e-m, Supplementary Figure S4c-h). All nine apical junctional proteins were found to be significantly downregulated. Such downregulation could be rescued using antioxidants such as catalase or SOD1 (Figure 4e-m, Supplementary Figure S4c-h).

KRT6A attenuated apical junctional proteins at the migration front

Keratin intermediate filament proteins are stress responsive and participate in host defense response (Zhang et al., 2019). Screening of keratins led to the identification of KRT6A as a pyocyanin-inducible protein (Figure 5a,b) in the keratinocyte with significance in cell migration. Overexpression of KRT6A (Figure 5c) accelerated cell migration (Figure 5d-g). The cell viability was comparable in both vehicle control and KRT6A over expressed cells (Supplementary Figure S5a-c). These observations assign cell migration support role to KRT6A.

KRT6A overexpression accelerated migration but it did so in a qualitatively deficient manner. Re-epithelialization dependent restoration of barrier function requires appropriate cell-cell sealing as afforded by the apical junctional proteins discussed above. Human keratinocyte KRT6A over-expression significantly depleted all these apical junctional proteins except JAM-A (Figure 5h-p, Supplementary Figure S5d-i).

Topical pyocyanin application accelerated reepithelialization in diabetic mice

Topical application of pyocyanin on diabetic wound every alternate day accelerated wound closure in diabetic mice (Figure 6a,b). Analytical histology confirmed significant improvement in wound closure displayed by db/db mice treated topically with pyocyanin (Figure 6c-e). No change in wound length or granulation tissue area were observed (Figure 6d). Immunohistochemical analysis of KRT6A showed significant increase in epithelial KRT6A expression (Figure 6f,g).

DISCUSSION

Under conditions of infection, virulence factors released by bacteria subvert host immune defenses (Casadevall and Pirofski, 2001, Lavoie et al., 2011, Sharma et al., 2017). Another common target in the host is mitochondrial metabolism (Boya et al., 2001, Hall et al., 2016, Kozjak-Pavlovic et al., 2008, Tiku et al., 2020). Induction of host mitochondrial dysfunction is often an early step towards infection-associated loss of tissue viability. Bacteria release mitochondrial toxins into the tissue microenvironment thus weakening

Author Manuscript
Author Manuscript
Author Manuscript

host defenses (Aguilar-Lopez et al., 2020, Han et al., 2019). Under such conditions of compromised mitochondrial, the lower energy yield path of aerobic glycolysis is induced as compensatory survival response (Tiku et al., 2020).

Pyocyanin, released by *Pseudomonas*, is blue in color when oxidized. It is a cell membrane permeable toxin that is pro-inflammatory and induces oxidative stress in host cell (Hall et al., 2016, Lau et al., 2004, Turner and Messenger, 1986). *Pseudomonas* infection is common in skin lesions where keratinocytes play an important role in host defense (Golovkine et al., 2016, Golovkine et al., 2018, Heiniger et al., 2010). In an experimental setting, seeking ratiometric quantitative data on a proteome-wide basis, SILAC is reported to be the most accurate MS-based approach (Bantscheff et al., 2007, Ong et al., 2002, Zhang et al., 2009). SILAC proteomic studies identified that two out of twelve pyocyanin-sensitive pathways were related to mitochondrial dysfunction and bioenergetics. Direct study of mitochondrial function revealed that pyocyanin exposure cause keratinocyte mitochondrial dysfunction and anergy. Under conditions of mitochondrial dysfunction, the expression of proteins relevant to oxidative phosphorylation is known to be upregulated (Danielson et al., 2005, Reinecke et al., 2009). Such compensatory response is often futile in recovering mitochondrial function.

The association of cellular ROS production with pyocyanin-induced mitochondrial dysfunction, as noted in this work, is explained by the inherent redox properties of pyocyanin (Hall et al., 2016, Manago et al., 2015). Pyocyanin stimulates cellular superoxide ($O_2^{\bullet -}$) production (Hall et al., 2016, Manago et al., 2015). This is directly evident from the electron paramagnetic resonance studies of this work. Elevated superoxide dismutates to cellular hydrogen peroxide (H_2O_2). Build-up of ROS within the cell is known to contribute to mitochondrial dysfunction and further elevate superoxide levels resulting in a vicious loop (Balaban et al., 2005). Oxidant loading within the cell oxidized glutathione lowering GSH/GSSG in response to pyocyanin exposure. Elevated GSSG is subject to the activity of GSSG reductase for the regeneration of GSH at the expense of NADPH. Thus, GSH oxidation consumes NADPH/NADP. Excessive cellular GSSG, beyond the cellular capacity to recycle, is cytotoxic and is therefore expelled from cells contributing to total glutathione depletion (Park et al., 2009). Findings of this work are consistent with prior work reporting on glutathione depletion in response to pyocyanin exposure (O'Malley et al., 2004). Lower NADPH levels are attributed to the downregulation of NADPH-generating pathways as observed in SILAC. Furthermore, bacterial infection activates oxidant-producing enzymes such as NADPH oxidase (NOX) which oxidizes NADPH to NADP and generates superoxide (Park et al., 2004; MontalvoJave et al., 2016). High cellular superoxide in response to pyocyanin may inhibit the pyruvate dehydrogenase complex and thus deplete cellular NADH (Price-Whelan et al., 2007).

Injury perturbs the status quo of terminal differentiation of keratinocytes preparing the cells to migrate (Sen and Roy, 2021). Intracellular organization of keratin intermediate filaments represents a major component of such preparation. Keratin intermediate filament proteins, including microfilaments and microtubules, make up the cytoskeleton of the cell and are stress responsive (Fuchs and Cleveland, 1998, Zhang et al., 2019). Type I and type II keratin proteins pair to form polymeric filaments which respond to their cellular environment. Recent works recognize KRT6/16/17 as key early barrier alarmins (Zhang et al., 2019). Upregulation of these keratins induce host defense response (Zhang et al., 2019). KRT6A and its type I partners (KRT16 or KRT17) are subject to both constitutive and inducible regulation. In resting healthy skin, KRT6A is localized between the inner root sheath and outer root sheath (ORS) of the hair follicle (Rothnagel and Roop, 1995). KRT6A is inducible in the ORS as well as in interfollicular keratinocytes by mechanical trauma, wounding, and other disease states (Mansbridge and Knapp, 1987, Stoler et al., 1988, Weiss et al., 1984). To our knowledge previously unreported, this work presents first evidence demonstrating that KRT6A is inducible in response to a bacterial product. Epithelial cell migration, which achieves re-epithelialization of defect, is energy dependent (Padhi et al., 2020). Glycolysis produces ATP rapidly with low-yield. Mitochondrial oxidative phosphorylation is more efficient but much slower. Studies on inhibition of these pathways have led to the observation that cell migration is predominantly powered by glycolysis than mitochondrial energetics (Arseneault et al., 2013, Mustafa et al., 2015). This explains why KRT6A is able to accelerate epithelial migration under conditions of mitochondrial dysfunction as noted in the current work. Topical pyocyanin application induced KRT6a expression in non-healing wounds of diabetic mice that resulted in faster reepithelialization. Thus, KRT6A may be viewed as a component of the acute host defense system that is able to sense bacterial products and accelerate wound closure. Our previous works have shown that restoration of epithelial closure in response to bacterial threat is associated with poor quality of tissue repair such that barrier function of the repaired skin remains impaired because of inadequate apical junctional proteins (Barki et al., 2019, Roy et al., 2014). In keratinocytes, apical junctional proteins seal the space between cells (DiTommaso et al., 2014). Apical junction proteins are made up of tight junctional and adherens junctional proteins. Tight junctions (TJ), transmembrane proteins *such as* claudins, occludin and junction adhesion molecule, form a seal between cells during re-epithelialization (Niessen, 2007). In addition, TJ associate with peripheral proteins such as ZO-1 (Stevenson et al., 1986) which in turn interacts with ZO-2 (Jesaitis and Goodenough, 1994) and ZO-3 (Haskins et al., 1998). TJ interacts with the intermediate filament network (Fanning et al., 1998). Compared to TJ, adherens junctions (AJ) are relatively basal in location and also form a zonula primarily composed of E-cadherin transmembrane proteins. Both TJ and AJ are targets of *P. aeruginosa*'s virulence factors (Golovkine et al., 2018). Consistently, this work demonstrates that pyocyanin exposure down-regulates TJ and AJ expression during keratinocyte migration. Of outstanding therapeutic interest is the observation that even under the absence of any bacterial virulence factor overexpression of KRT6A alone is sufficient to blunt both TJ as well as AJ expression in keratinocytes with accelerated migration.

Pyocyanin is released by bacteria into body fluids and can access tissue sites remote from the actual site of infection. It has potent inhibitory action on tissue mitochondrial function subduing host defense factors thus paving the way for spread of infection. Findings of this work recognize KRT6A, type II intermediate filament, as an acute host defense factor that is pyocyanin-sensitive. Once alarmed by the bacterial threat, elevated KRT6A is capable of markedly accelerating keratinocyte migration. Closure of the defect, thus achieved, is rapid but qualitatively compromised by down-regulated expression of junctional proteins. These mechanistic insights explain why an infected wound close with deficient skin barrier function as evident *in vivo* (Barki et al., 2019, Roy et al., 2014, Roy et al., 2020).

MATERIALS AND METHODS

Cell lines

Human keratinocytes (HaCaT) were cultured in low D-glucose DMEM medium supplemented with 10% FBS and 100 U/ml penicillin and 100 μg/ml streptomycin at 37°C and 5% CO_2.

Animals and Wound Models

Mice homozygous (db/db; stock no 000642) for spontaneous mutation of the leptin receptor or their respective non-diabetic lean control littermates m^+/db (aged 10–12 weeks) that serves as an established model for impaired healing (Chan et al., 2012) were obtained from Jackson Laboratory. All animal studies were performed in accordance with protocols approved by the Laboratory Animal Resource Center of Indiana University. Full-thickness excisional wounds were developed on the dorsal skin of mice as reported previously (Chen et al., 2009, Chen et al., 2008, Ghatak et al., 2015, Wu et al., 2007). Wound area was calculated using digital planimetry (Das et al., 2016).

Immunocytochemistry, Immunohistochemistry, Microscopy and Histomorphometric analysis

Immunocytochemistry and immunohistochemistry were performed using antibodies against DRP1 (Abcam, Cat # ab184247, 1:500), OPA1 (Abcam, Cat # ab157457, 1:200), Occludin (Invitrogen, 71–1500; 1:200), ZO-1 (Invitrogen, 61–7300; 1:200), ZO-2 (Invitrogen, 38–9100; 1:200), Claudin1 (Invitrogen, 51–9000; 1:100), Claudin 4 (Invitrogen, 32–9400; 1:250), β-catenin (Abcam, ab32572, 1:500), e-cadherin (Invitrogen, MA5–12547; 1:200), tricellulin (Invitrogen, 48–8400; 1:250), JAM-A (Invitrogen, 36–1700; 1:50), KRT6A (Abcam, Cat # ab238013, 1:500), and KRT14 (BioLegend, Cat # 905301, 1:400) as reported previously (Ahmed et al., 2017, Clark et al., 2022, Li et al., 2018, Zhou et al., 2020). All images were captured using CLSM (Zeiss LSM 880) microscope. Fluorescence signal intensity quantitation was performed using ZEN 3.0 (Zeiss) software. The extent of epithelialization and granulation tissue formation was determined on H&E-stained paraffin tissue sections as reported (Eming et al., 2007, Gerharz et al., 2007, Ghatak et al., 2022, Lucas et al., 2010).

SILAC labeling

In vitro SILAC labeling, protein extraction, proteomics and computational analysis were performed as reported by us previously (Singh et al., 2017, Singh et al., 2019). The ratios between heavy and light isotope labeling for each identified protein were calculated using

Mitochondrial assays in human keratinocytes

Mitochondrial stress was measured with Sea Horse XFe96 Analyzer as reported previously (Ghatak et al., 2022). Mitochondrial $O_2^{-\cdot}$ abundance and membrane potential were measured with MitoSOX red and JC-1 dye respectively. ATP/ADP ratio was measured using luciferin-luciferase reaction based EnzyLight ATP/ADP ratio assay kit (BioAssay Systems, Hayward, CA, USA.) according to the manufacturer's instructions. Mitochondria network morphology analysis was performed from cells stained with mitotracker red using ImageJ macro toolset (MiNA) (Valente et al., 2017).

EPR spectroscopy and spin trapping of ROS

ROS in human keratinocytes were measured by electron paramagnetic resonance (EPR) spin trapping using Bruker EMXplus X-band spectrometer equipped with an HS (high-sensitivity) resonator. EPR spectra were quantitated by double integration using Bruker WinEPR Version 2.11 by comparison with 4-oxo-2,2,6,6-tetramethyl-1-piperidinyloxy (4-oxo-TEMPO) as a standard as reported previously (Lee et al., 2014).

Lactate assay

Cellular lactate levels were measured using colorimetric L-lactate assay kit (abcam, ab65331) as per manufacture's instruction (Vollmers et al., 2021, Zheng et al., 2021).

Cytosolic $O_2^{-\cdot}$ and H_2O_2 abundance in human keratinocytes

Cytosolic $O_2^{-\cdot}$ and H_2O_2 abundance were measured with dihydroethidium (DHE) fluorescent probe and pHyPer-cyto respectively.

HPLC analysis of NAD(P)H and glutathione

HPLC coupled to fluorescence spectroscopy was used to analyze cellular NAD(P)H content, reduced (GSH) and oxidized (GSSG) glutathione.

Keratinocyte's migration

Keratinocyte migration assay was performed using silicone cell culture insert (Ibidi, Fitchburg, WI) as described previously (Banerjee et al., 2014, Ghatak et al., 2022).

KRT6A ELISA

KRT6A levels were measured in human keratinocytes after KRT6A over-expression for 48h as per manufacturer's instructions (MyBiosource.com).

Quantification and Statistical Analysis

The data are presented as mean ± standard deviation. Comparisons between the two groups were statistically evaluated by Welch's t-test. Comparisons between two and more groups were statistically evaluated by one-way ANOVA (one independent variable) or two-way ANOVA (two or more independent variables). The statistical evaluation was done using GraphPad Prism (version 8). A *P-value* ≤ 0.05 was considered statistically significant.

Supplementary Material

Refer to Web version on PubMed Central for supplementary material.

ACKNOWLEDGEMENTS

Karamjeet Kaur, Ph.D, was credited as the first author in the original submission but had to be removed in consultation with the journal office because she could not be contacted for author consent after her return to India. This work was supported by National Institutes of Health R01 grants NR013898 and DK125835 to CKS. This work was also supported by a Lilly INCITE scholar fund awarded to CKS. We thank Liwen Zhang (Proteomic Shared Resources, The Ohio State University) for her help in LC-MS/MS. The Fusion Orbitrap instrument was supported by NIH grant S10 OD018056.

Data and Code Availability

Datasets related to this article can be found at https://massive.ucsd.edu/ProteoSAFe/dataset.jsp?task=d3ee2f0b9ebf4c11912171d37534a492, hosted at MassIVE database (Accession number MSV000091054). The mass spectrometry proteomics data generated during this study is uploaded in and also available in Supplementary Files 1 and 2.

Abbreviations

A+R	Antimycin+Rotenone
CAT	catalase
CCCP	carbonyl cyanide m-chlorophenyl hydrazine
DAPI	4′,6-diamidino-2-phenylindole
ECAR	Extracellular acidification rate
KRT6A	Keratin 6A
OE	over-expression
MnTBAP	Mn(III) tetrakis (4-benzoic acid) porphyrin chloride
OCR	oxygen consumption rate
PYO	pyocyanin
SOD	superoxide dismutase

REFERENCES

Aguilar-Lopez BA, Moreno-Altamirano MMB, Dockrell HM, Duchen MR, Sanchez-Garcia FJ. Mitochondria: An Integrative Hub Coordinating Circadian Rhythms, Metabolism, the Microbiome, and Immunity. Front Cell Dev Biol 2020;8:51. [PubMed: 32117978]

Ahmed NS, Ghatak S, El Masry MS, Gnyawali SC, Roy S, Amer M, et al. Epidermal E-Cadherin Dependent β-Catenin Pathway Is Phytochemical Inducible and Accelerates Anagen Hair Cycling. Mol Ther 2017;25(11):2502–12. [PubMed: 28803863]

Arseneault R, Chien A, Newington JT, Rappon T, Harris R, Cumming RC. Attenuation of LDHA expression in cancer cells leads to redox-dependent alterations in cytoskeletal structure and cell migration. Cancer Lett 2013;338(2):255–66. [PubMed: 23583676]

Balaban RS, Nemoto S, Finkel T. Mitochondria, oxidants, and aging. Cell 2005;120(4):483–95. [PubMed: 15734681]

Banerjee J, Das Ghatak P, Roy S, Khanna S, Sequin EK, Bellman K, et al. Improvement of human keratinocyte migration by a redox active bioelectric dressing. PloS one 2014;9(3):e89239-e.

Bantscheff M, Schirle M, Sweetman G, Rick J, Kuster B. Quantitative mass spectrometry in proteomics: a critical review. Anal Bioanal Chem 2007;389(4):1017–31. [PubMed: 17668192]

Barki KG, Das A, Dixith S, Ghatak PD, Mathew-Steiner S, Schwab E, et al. Electric Field Based Dressing Disrupts Mixed-Species Bacterial Biofilm Infection and Restores Functional Wound Healing. Ann Surg 2019;269(4):756–66. [PubMed: 29099398]

Belousov VV, Fradkov AF, Lukyanov KA, Staroverov DB, Shakhbazov KS, Terskikh AV, et al. Genetically encoded fluorescent indicator for intracellular hydrogen peroxide. Nat Methods 2006;3(4):281–6. [PubMed: 16554833]

Boya P, Roques B, Kroemer G. New EMBO members' review: viral and bacterial proteins regulating apoptosis at the mitochondrial level. EMBO J 2001;20(16):4325–31. [PubMed: 11500358]

Casadevall A, Pirofski L. Host-pathogen interactions: the attributes of virulence. J Infect Dis 2001;184(3):337–44. [PubMed: 11443560]

Chan YC, Roy S, Khanna S, Sen CK. Downregulation of endothelial microRNA-200b supports cutaneous wound angiogenesis by desilencing GATA binding protein 2 and vascular endothelial growth factor receptor 2. Arteriosclerosis, thrombosis, and vascular biology 2012;32(6):1372–82. [PubMed: 22499991]

Chen L, Tredget EE, Liu C, Wu Y. Analysis of allogenicity of mesenchymal stem cells in engraftment and wound healing in mice. PloS one 2009;4(9):e7119. [PubMed: 19771171]

Chen L, Tredget EE, Wu PY, Wu Y. Paracrine factors of mesenchymal stem cells recruit macrophages and endothelial lineage cells and enhance wound healing. PloS one 2008;3(4):e1886. [PubMed: 18382669]

Clark A, Ghatak S, Guda PR, El Masry MS, Xuan Y, Sato AY, et al. Myogenic tissue nanotransfection improves muscle torque recovery following volumetric muscle loss. NPJ Regen Med 2022;7(1):63. [PubMed: 36266362]

Cruickshank CN, Lowbury EJ. The effect of pyocyanin on human skin cells and leucocytes. Br J Exp Pathol 1953;34(6):583–7. [PubMed: 13115587]

Danielson SR, Carelli V, Tan G, Martinuzzi A, Schapira AH, Savontaus ML, et al. Isolation of transcriptomal changes attributable to LHON mutations and the cybridization process. Brain 2005;128(Pt 5):1026–37. [PubMed: 15728653]

Das A, Ghatak S, Sinha M, Chaffee S, Ahmed NS, Parinandi NL, et al. Correction of MFG-E8 Resolves Inflammation and Promotes Cutaneous Wound Healing in Diabetes. J Immunol 2016;196(12):5089–100. [PubMed: 27194784]

Deng B, Ghatak S, Sarkar S, Singh K, Das Ghatak P, Mathew-Steiner SS, et al. Novel Bacterial Diversity and Fragmented eDNA Identified in Hyperbiofilm-Forming Pseudomonas aeruginosa Rugose Small Colony Variant. iScience 2020;23(2):100827. [PubMed: 32058950]

DiTommaso T, Cottle DL, Pearson HB, Schluter H, Kaur P, Humbert PO, et al. Keratin 76 is required for tight junction function and maintenance of the skin barrier. PLoS Genet 2014;10(10):e1004706. [PubMed: 25340345]

Eming SA, Werner S, Bugnon P, Wickenhauser C, Siewe L, Utermöhlen O, et al. Accelerated wound closure in mice deficient for interleukin-10. Am J Pathol 2007;170(1):188–202. [PubMed: 17200193]

Fanning AS, Jameson BJ, Jesaitis LA, Anderson JM. The tight junction protein ZO-1 establishes a link between the transmembrane protein occludin and the actin cytoskeleton. J Biol Chem 1998;273(45):29745–53. [PubMed: 9792688]

Flemming HC, Wingender J. The biofilm matrix. Nat Rev Microbiol 2010;8(9):623–33. [PubMed: 20676145]

Fuchs E, Cleveland DW. A structural scaffolding of intermediate filaments in health and disease. Science 1998;279(5350):514–9. [PubMed: 9438837]

Gerharz M, Baranowsky A, Siebolts U, Eming S, Nischt R, Krieg T, et al. Morphometric analysis of murine skin wound healing: standardization of experimental procedures and impact of an advanced multitissue array technique. Wound Repair Regen 2007;15(1):105–12. [PubMed: 17244326]

Ghatak S, Chan YC, Khanna S, Banerjee J, Weist J, Roy S, et al. Barrier Function of the Repaired Skin Is Disrupted Following Arrest of Dicer in Keratinocytes. Mol Ther 2015;23(7):1201–10. [PubMed: 25896246]

Ghatak S, Khanna S, Roy S, Thirunavukkarasu M, Pradeep SR, Wulff BC, et al. Driving adult tissue repair via re-engagement of a pathway required for fetal healing. Mol Ther 2022.

Golovkine G, Faudry E, Bouillot S, Elsen S, Attree I, Huber P. Pseudomonas aeruginosa Transmigrates at Epithelial Cell-Cell Junctions, Exploiting Sites of Cell Division and Senescent Cell Extrusion. PLoS Pathog 2016;12(1):e1005377. [PubMed: 26727615]

Golovkine G, Reboud E, Huber P. Corrigendum: Pseudomonas aeruginosa Takes a Multi-Target Approach to Achieve Junction Breach. Front Cell Infect Microbiol 2018;8:52. [PubMed: 29569635]

Hall S, McDermott C, Anoopkumar-Dukie S, McFarland AJ, Forbes A, Perkins AV, et al. Cellular Effects of Pyocyanin, a Secreted Virulence Factor of Pseudomonas aeruginosa. Toxins (Basel) 2016;8(8).

Han B, Lin CJ, Hu G, Wang MC. ‘Inside Out’- a dialogue between mitochondria and bacteria. FEBS J 2019;286(4):630–41. [PubMed: 30390412]

Haskins J, Gu L, Wittchen ES, Hibbard J, Stevenson BR. ZO-3, a novel member of the MAGUK protein family found at the tight junction, interacts with ZO-1 and occludin. J Cell Biol 1998;141(1):199–208. [PubMed: 9531559]

Heiniger RW, Winther-Larsen HC, Pickles RJ, Koomey M, Wolfgang MC. Infection of human mucosal tissue by Pseudomonas aeruginosa requires sequential and mutually dependent virulence factors and a novel pilus-associated adhesin. Cell Microbiol 2010;12(8):1158–73. [PubMed: 20331639]

Jastroch M, Divakaruni AS, Mookerjee S, Treberg JR, Brand MD. Mitochondrial proton and electron leaks. Essays Biochem 2010;47:53–67. [PubMed: 20533900]

Jesaitis LA, Goodenough DA. Molecular characterization and tissue distribution of ZO-2, a tight junction protein homologous to ZO-1 and the Drosophila discs-large tumor suppressor protein. J Cell Biol 1994;124(6):949–61. [PubMed: 8132716]

Kozjak-Pavlovic V, Ross K, Rudel T. Import of bacterial pathogenicity factors into mitochondria. Curr Opin Microbiol 2008;11(1):9–14. [PubMed: 18280201]

Lau GW, Hassett DJ, Ran H, Kong F. The role of pyocyanin in Pseudomonas aeruginosa infection. Trends Mol Med 2004;10(12):599–606. [PubMed: 15567330]

Lavoie EG, Wangdi T, Kazmierczak BI. Innate immune responses to Pseudomonas aeruginosa infection. Microbes Infect 2011;13(14–15):1133–45. [PubMed: 21839853]

Lee MC, Velayutham M, Komatsu T, Hille R, Zweier JL. Measurement and characterization of superoxide generation from xanthine dehydrogenase: a redox-regulated pathway of radical generation in ischemic tissues. Biochemistry 2014;53(41):6615–23. [PubMed: 25243829]

Li J, Ghatak S, El Masry MS, Das A, Liu Y, Roy S, et al. Topical Lyophilized Targeted Lipid Nanoparticles in the Restoration of Skin Barrier Function following Burn Wound. Mol Ther 2018;26(9):2178–88. [PubMed: 29802017]

Lucas T, Waisman A, Ranjan R, Roes J, Krieg T, Müller W, et al. Differential roles of macrophages in diverse phases of skin repair. J Immunol 2010;184(7):3964–77. [PubMed: 20176743]

Mahajan-Miklos S, Tan MW, Rahme LG, Ausubel FM. Molecular mechanisms of bacterial virulence elucidated using a Pseudomonas aeruginosa-Caenorhabditis elegans pathogenesis model. Cell 1999;96(1):47–56. [PubMed: 9989496]

Manago A, Becker KA, Carpinteiro A, Wilker B, Soddemann M, Seitz AP, et al. Pseudomonas aeruginosa pyocyanin induces neutrophil death via mitochondrial reactive oxygen species and mitochondrial acid sphingomyelinase. Antioxid Redox Signal 2015;22(13):1097–110. [PubMed: 25686490]

Mansbridge JN, Knapp AM. Changes in keratinocyte maturation during wound healing. J Invest Dermatol 1987;89(3):253–63. [PubMed: 2442269]

Mihai MM, Holban AM, Giurcaneanu C, Popa LG, Buzea M, Filipov M, et al. Identification and phenotypic characterization of the most frequent bacterial etiologies in chronic skin ulcers. Rom J Morphol Embryol 2014;55(4):1401–8. [PubMed: 25611273]

Mittal R, Aggarwal S, Sharma S, Chhibber S, Harjai K. Urinary tract infections caused by Pseudomonas aeruginosa: a minireview. J Infect Public Health 2009;2(3):101–11. [PubMed: 20701869]

Muller M. Premature cellular senescence induced by pyocyanin, a redox-active Pseudomonas aeruginosa toxin. Free Radic Biol Med 2006;41(11):1670–7. [PubMed: 17145555]

Mustafa EH, Mahmoud HT, Al-Hudhud MY, Abdalla MY, Ahmad IM, Yasin SR, et al. 2-deoxy-D-Glucose Synergizes with Doxorubicin or L-Buthionine Sulfoximine to Reduce Adhesion and Migration of Breast Cancer Cells. Asian Pac J Cancer Prev 2015;16(8):3213–22. [PubMed: 25921122]

Niessen CM. Tight junctions/adherens junctions: basic structure and function. J Invest Dermatol 2007;127(11):2525–32. [PubMed: 17934504]

Norbury W, Herndon DN, Tanksley J, Jeschke MG, Finnerty CC. Infection in Burns. Surg Infect (Larchmt) 2016;17(2):250–5. [PubMed: 26978531]

O'Malley YQ, Reszka KJ, Spitz DR, Denning GM, Britigan BE. Pseudomonas aeruginosa pyocyanin directly oxidizes glutathione and decreases its levels in airway epithelial cells. Am J Physiol Lung Cell Mol Physiol 2004;287(1):L94–103. [PubMed: 15020296]

Ong SE, Blagoev B, Kratchmarova I, Kristensen DB, Steen H, Pandey A, et al. Stable isotope labeling by amino acids in cell culture, SILAC, as a simple and accurate approach to expression proteomics. Mol Cell Proteomics 2002;1(5):376–86. [PubMed: 12118079]

Padhi A, Thomson AH, Perry JB, Davis GN, McMillan RP, Loesgen S, et al. Bioenergetics underlying single-cell migration on aligned nanofiber scaffolds. Am J Physiol Cell Physiol 2020;318(3):C476–C85. [PubMed: 31875698]

Park HA, Khanna S, Rink C, Gnyawali S, Roy S, Sen CK. Glutathione disulfide induces neural cell death via a 12-lipoxygenase pathway. Cell Death Differ 2009;16(8):1167–79. [PubMed: 19373248]

Price-Whelan A, Dietrich LE, Newman DK. Pyocyanin alters redox homeostasis and carbon flux through central metabolic pathways in Pseudomonas aeruginosa PA14. J Bacteriol 2007;189(17):6372–81. [PubMed: 17526704]

Reimer A, Edvaller B, Johansson B. Concentrations of the Pseudomonas aeruginosa toxin pyocyanin in human ear secretions. Acta Otolaryngol Suppl 2000;543:86–8. [PubMed: 10908987]

Reinecke F, Smeitink JA, van der Westhuizen FH. OXPHOS gene expression and control in mitochondrial disorders. Biochim Biophys Acta 2009;1792(12):1113–21. [PubMed: 19389473]

Rothnagel JA, Roop DR. Hair follicle companion layer: reacquainting an old friend. J Invest Dermatol 1995;104(5 Suppl):42S–3S. [PubMed: 7537786]

Roy S, Elgharably H, Sinha M, Ganesh K, Chaney S, Mann E, et al. Mixed-species biofilm compromises wound healing by disrupting epidermal barrier function. J Pathol 2014;233(4):331–43. [PubMed: 24771509]

Roy S, Santra S, Das A, Dixith S, Sinha M, Ghatak S, et al. Staphylococcus aureus Biofilm Infection Compromises Wound Healing by Causing Deficiencies in Granulation Tissue Collagen. Ann Surg 2020;271(6):1174–85. [PubMed: 30614873]

Ruffin M, Brochiero E. Repair Process Impairment by Pseudomonas aeruginosa in Epithelial Tissues: Major Features and Potential Therapeutic Avenues. Front Cell Infect Microbiol 2019;9:182. [PubMed: 31214514]

Sen CK, Roy S. The Hyperglycemia Stranglehold Stifles Cutaneous Epithelial−Mesenchymal Plasticity and Functional Wound Closure. J Invest Dermatol 2021;141(6):1382–5. [PubMed: 34024339]

Sharma AK, Dhasmana N, Dubey N, Kumar N, Gangwal A, Gupta M, et al. Bacterial Virulence Factors: Secreted for Survival. Indian J Microbiol 2017;57(1):1–10. [PubMed: 28148975]

Singh K, Pal D, Sinha M, Ghatak S, Gnyawali SC, Khanna S, et al. Epigenetic Modification of MicroRNA-200b Contributes to Diabetic Vasculopathy. Mol Ther 2017;25(12):2689–704. [PubMed: 29037594]

Singh K, Sinha M, Pal D, Tabasum S, Gnyawali SC, Khona D, et al. Cutaneous Epithelial to Mesenchymal Transition Activator ZEB1 Regulates Wound Angiogenesis and Closure in a Glycemic Status-Dependent Manner. Diabetes 2019;68(11):2175–90. [PubMed: 31439646]

Stevenson BR, Siliciano JD, Mooseker MS, Goodenough DA. Identification of ZO-1: a high molecular weight polypeptide associated with the tight junction (zonula occludens) in a variety of epithelia. J Cell Biol 1986;103(3):755–66. [PubMed: 3528172]

Stoler A, Kopan R, Duvic M, Fuchs E. Use of monospecific antisera and cRNA probes to localize the major changes in keratin expression during normal and abnormal epidermal differentiation. J Cell Biol 1988;107(2):427–46. [PubMed: 2458356]

Tiku V, Tan MW, Dikic I. Mitochondrial Functions in Infection and Immunity. Trends Cell Biol 2020;30(4):263–75. [PubMed: 32200805]

Turner JM, Messenger AJ. Occurrence, biochemistry and physiology of phenazine pigment production. Adv Microb Physiol 1986;27:211–75. [PubMed: 3532716]

Valente AJ, Maddalena LA, Robb EL, Moradi F, Stuart JA. A simple ImageJ macro tool for analyzing mitochondrial network morphology in mammalian cell culture. Acta Histochem 2017;119(3):315–26. [PubMed: 28314612]

Van der Berg JP, Velema WA, Szymanski W, Driessen AJM, Feringa BL. Controlling the activity of quorum sensing autoinducers with light. Chem Sci 2015;6(6):3593–8. [PubMed: 29511521]

Vollmers AC, Covarrubias S, Kuang D, Shulkin A, Iwuagwu J, Katzman S, et al. A conserved long noncoding RNA, GAPLINC, modulates the immune response during endotoxic shock. Proc Natl Acad Sci U S A 2021;118(7).

Weiss RA, Eichner R, Sun TT. Monoclonal antibody analysis of keratin expression in epidermal diseases: a 48- and 56-kdalton keratin as molecular markers for hyperproliferative keratinocytes. J Cell Biol 1984;98(4):1397–406. [PubMed: 6201492]

Wilson R, Sykes DA, Watson D, Rutman A, Taylor GW, Cole PJ. Measurement of Pseudomonas aeruginosa phenazine pigments in sputum and assessment of their contribution to sputum sol toxicity for respiratory epithelium. Infect Immun 1988;56(9):2515–7. [PubMed: 3137173]

Wu Y, Chen L, Scott PG, Tredget EE. Mesenchymal stem cells enhance wound healing through differentiation and angiogenesis. Stem cells 2007;25(10):2648–59. [PubMed: 17615264]

Zhang G, Fenyo D, Neubert TA. Evaluation of the variation in sample preparation for comparative proteomics using stable isotope labeling by amino acids in cell culture. J Proteome Res 2009;8(3):1285–92. [PubMed: 19140678]

Zhang X, Yin M, Zhang LJ. Keratin 6, 16 and 17-Critical Barrier Alarmin Molecules in Skin Wounds and Psoriasis. Cells 2019;8(8).

Zheng F, Chen J, Zhang X, Wang Z, Chen J, Lin X, et al. The HIF-1α antisense long non-coding RNA drives a positive feedback loop of HIF-1α mediated transactivation and glycolysis. Nat Commun 2021;12(1):1341. [PubMed: 33637716]

Zhou X, Brown BA, Siegel AP, El Masry MS, Zeng X, Song W, et al. Exosome-Mediated Crosstalk between Keratinocytes and Macrophages in Cutaneous Wound Healing. ACS Nano 2020;14(10):12732–48. [PubMed: 32931251]

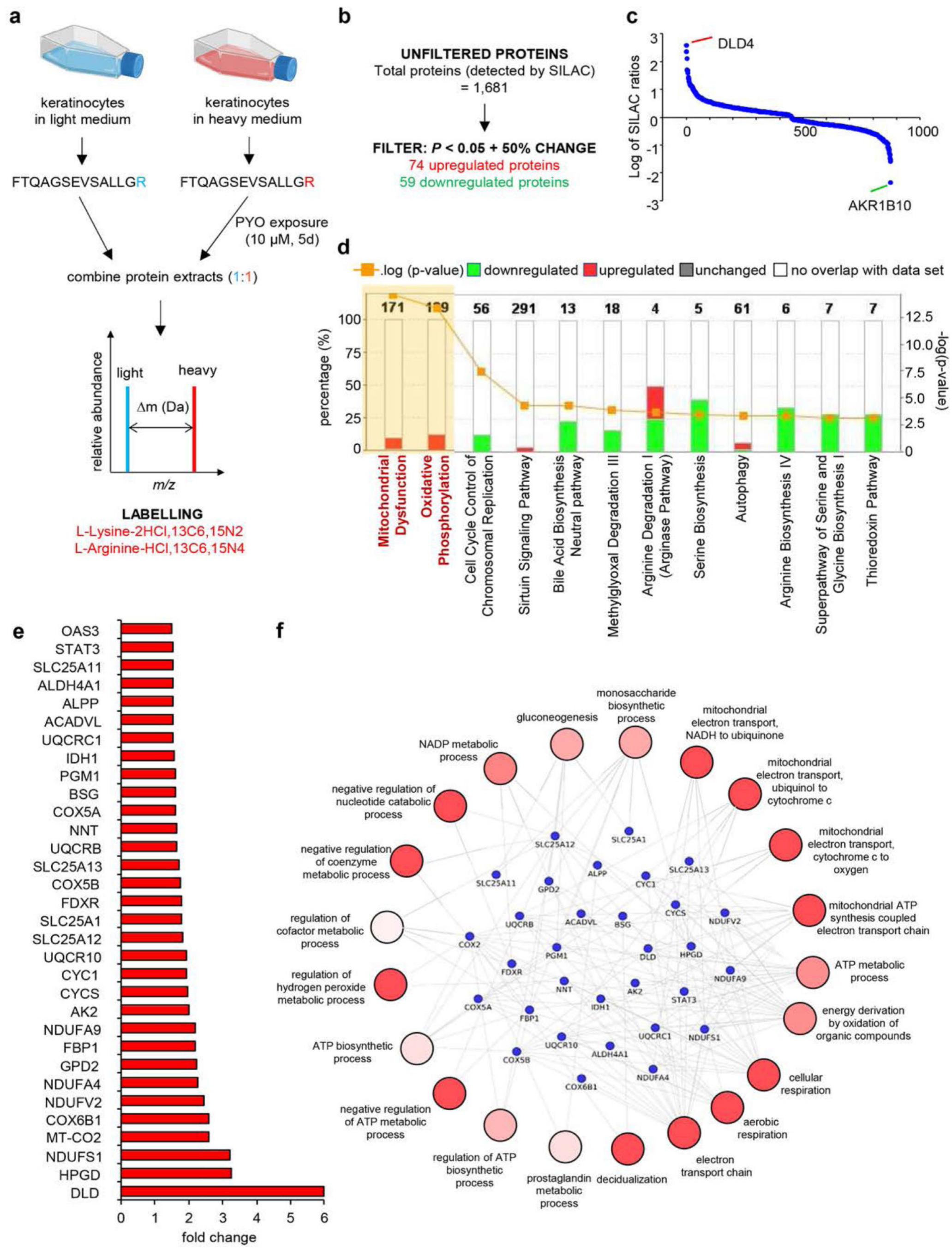

Figure 1. Bacterial pyocyanin targets mitochondrial proteins in human keratinocytes: SILAC quantitative proteomics.

(**a**) SILAC (stable isotope labeling with amino acids in cell culture) workflow. (**b**) Data mining strategy. (**c**) Log ratio distribution of differentially expressed proteins (DEPs) (p<0.05). (**d**) Ingenuity pathway analysis (IPA) of DEPs. Stacked bar chart showing canonical pathways associated with PYO exposure. Twelve candidate pathways having a -log (p-value) greater than 3 are displayed. (**e**) Up-regulated DEPs showing a minimum 50% change. (**f**) Gene Ontology enrichment of biological processes was performed on upregulated proteins *via* ClueGo app v.2.5.3 (Cytoscape plug-in). Enrichment criteria involved detection of at least two proteins/enrichment term. PYO exposure up-regulated the pathways relevant to cell metabolism and mitochondrial dysfunction. n=4.

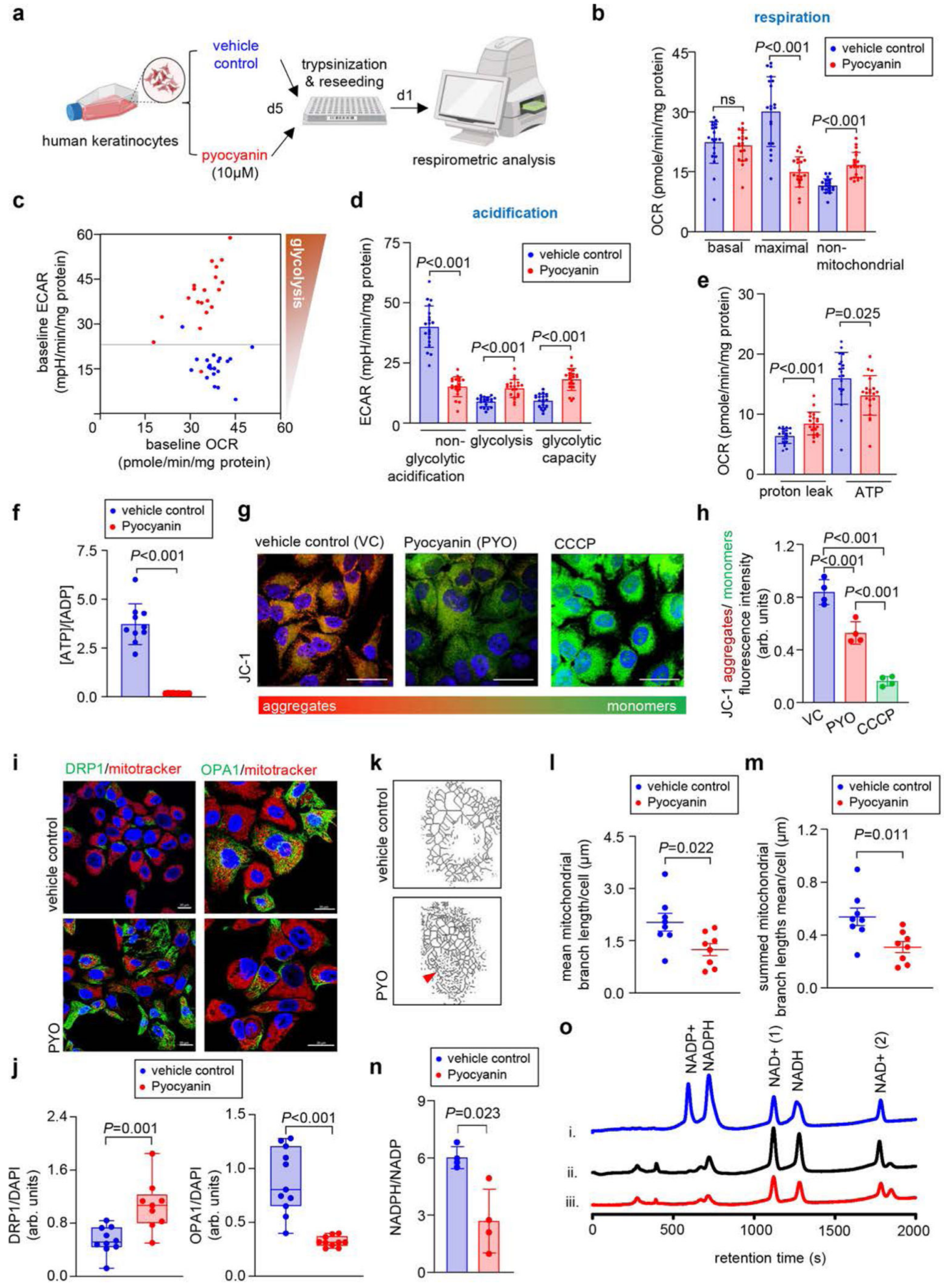

Figure 2. Pyocyanin compromised mitochondrial function in human keratinocytes with resultant decline in NAD(P)H and ATP levels.

(**a**) Schematic experimental design. (**b**) Baseline OCR and ECAR in human keratinocytes exposed to pyocyanin (red dots) or vehicle control (blue dots) was plotted graphically. (**c**) Mitochondrial functional assay after PYO exposure; n=15 as calculated from OCR. (**d**) Cellular acidification in vehicle control and pyocyanin exposed group as calculated from ECAR. n=15 (**e**) Proton leak and ATP content after PYO exposure; n=15 as calculated from OCR. (**f**) ATP/ADP ratio; n=10. (**g**) JC-1 aggregates:JC-1 monomers expression in human keratinocytes before and after PYO exposure (10 µM, 5d). Cells exposed to CCCP were used as positive control. Abundance of JC-1 monomers indicates highly depolarized mitochondrial membrane. Scale, 10 µm. (**h**) Quantification of JC-1 aggregates/monomers; n=6. (**i**) Representative immunocytochemistry of DRP1 and OPA1 costained with mitotracker red and DAPI. Scale, 20 µm. (**j**) Quantification of DRP1 and OPA1 intensity normalized with DAPI. n= 9,10. (**k**) Mitochondria morphology analysis using Mitochondria Network Analysis tool (MiNA) on ImageJ interface showing the skeletonized images of the fragmented mitochondria (red arrowhead). (**l-m**) Quantification of mean mitochondrial branch length (l) and summed mitochondrial branch lengths mean (m) per cell were plotted graphically. (n = 8) (**m**) NADPH/NADP ratio; n=4. (**c**) HPLC-Fluorescence chromatograms of NAD(P)(H). All data expressed as mean ± S.D. Data in h were analyzed using one-way ANOVA. Data in c, d, e, f, j, l, m, and n were analyzed by Student’s t test.

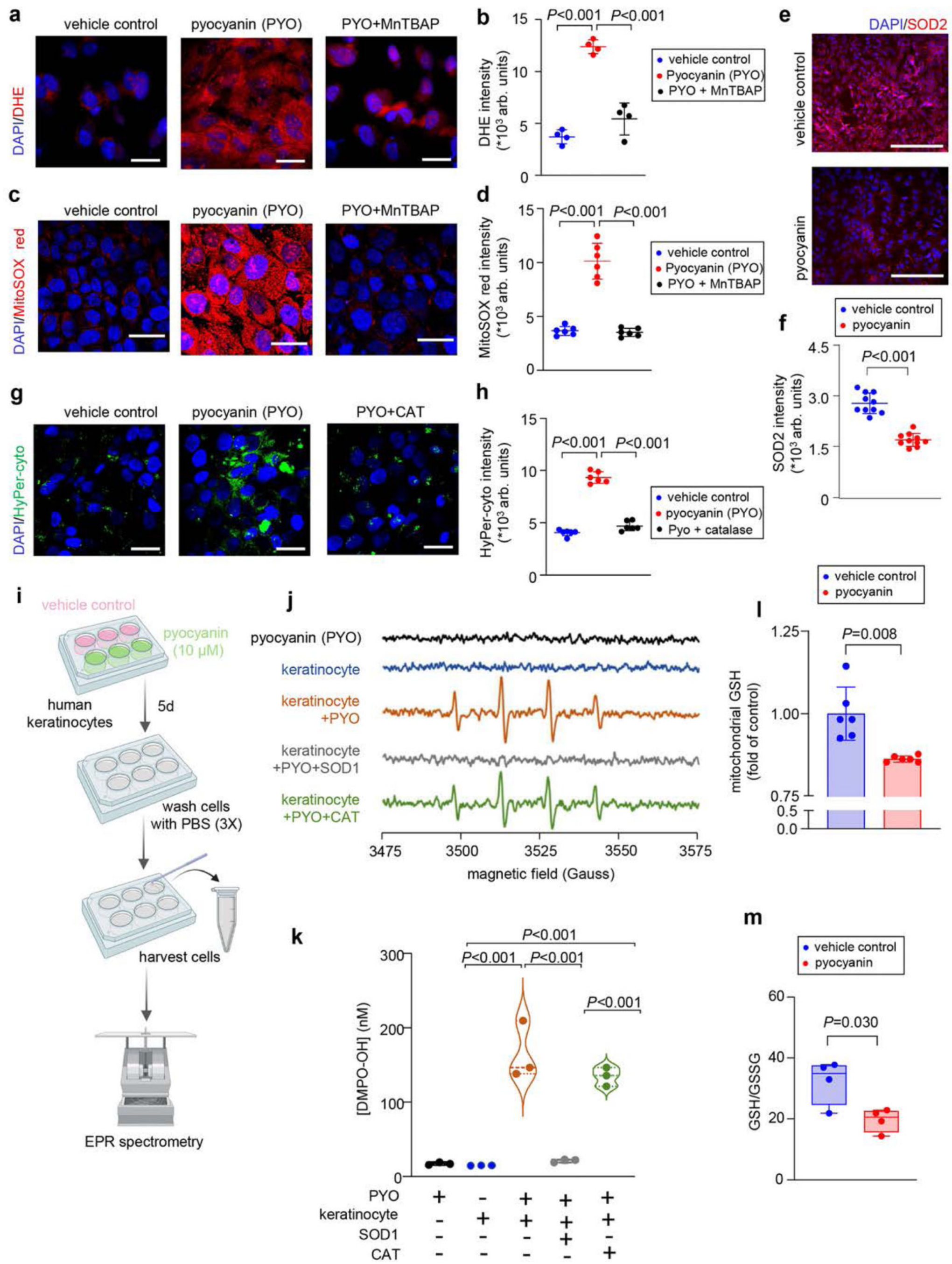

Figure 3. Pyocyanin induced oxygen centered free radicals generation in human keratinocytes and depleted cellular glutathione levels.

(**a-d**) Cellular and Mitochondrial superoxide detection (**a, c**) and quantification (**b, d**) in human keratinocytes after PYO exposure (10 µM, 5 d) using Dihydroethidium and MitoSOX red stain. Scale, 10 µm. n=6–4. (**e-f**) SOD2 expression (e) and quantification (f) following PYO exposure (10 µM, 5 d); scale,100 µm; n=10. (**g-h**) Cellular H_2O_2 detection (g) using HyPer-cyto and quantification (h) Scale, 10 µm; n=6,4. (**i**) Schematic experimental design for measuring ROS in human keratinocytes using EPR spectroscopy. (**j**) EPR spectra. (**k**)

Quantification of DMPO-OH species; n=3 (**l**) Mitochondrial GSH level. n=6. (**m**) GSH/GSSG ratio; n=4. All data expressed as mean ± S.D. Data in b,d, h and k were analyzed using one-way ANOVA. Data in f, l, and m were analyzed by Student's t test.

Author Manuscript
Author Manuscript
Author Manuscript

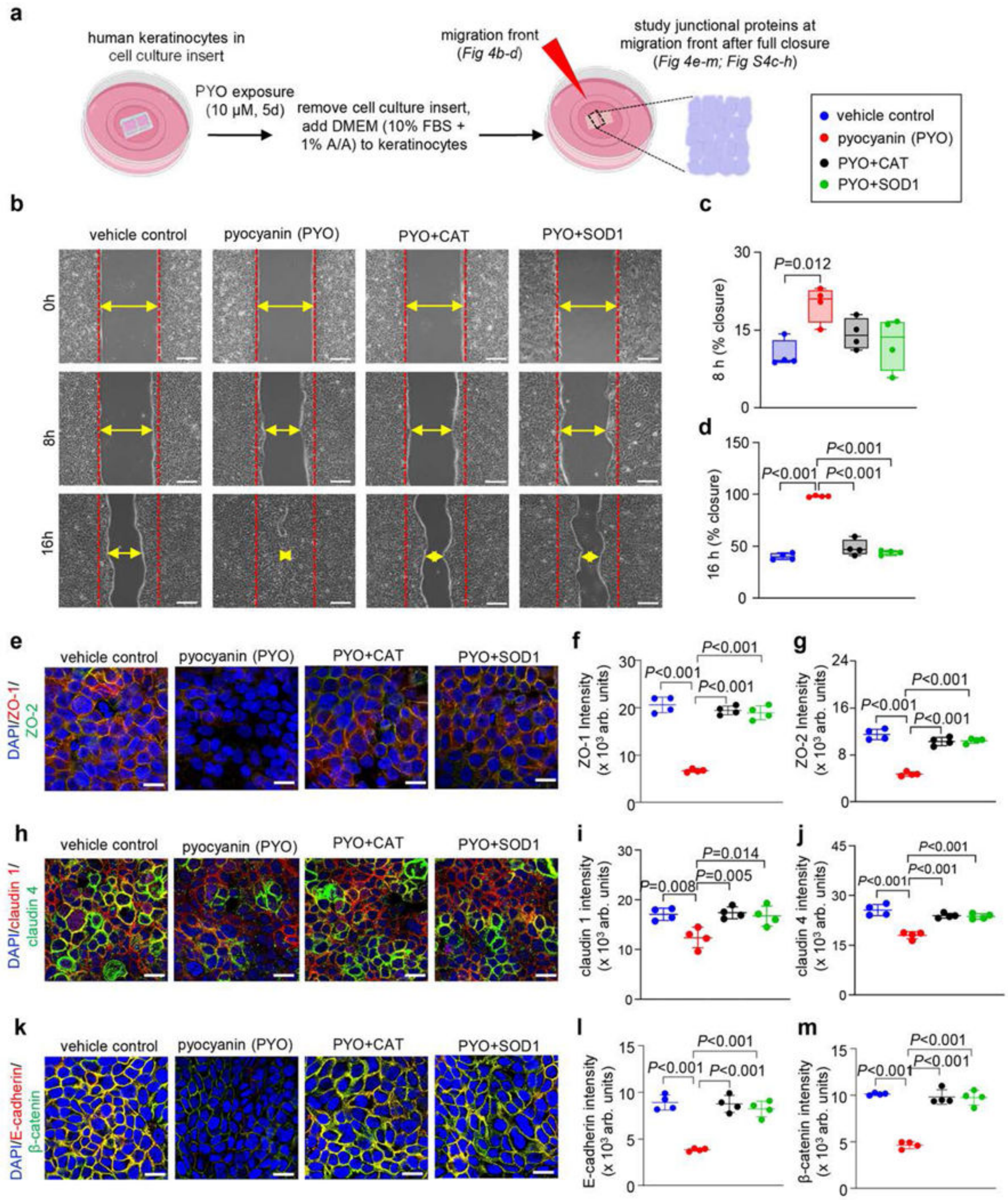

Figure 4. Pyocyanin induced accelerated human keratinocyte migration

(**a**) Schematic experimental design. (**b**) Keratinocyte migration at 0, 8 and 16 h with CAT (200 U) and SOD 1 (200U). scale, 200 μm. (**c**) Closure (%) in 8h. (**d**) Closure (%) in 16h; n=4. (**e-m**) Abundance of apical junctional proteins in response to PYO were measured using immunocytochemistry followed by quantitation; n=4 (mean ± SD). ZO-1: zonula occludens 1; ZO-2: zonula occludens 2; Scale, 10 μm. All data expressed as mean ± S.D. and were analyzed using one-way ANOVA. Data in f, l, and m were analyzed by Student's t test.

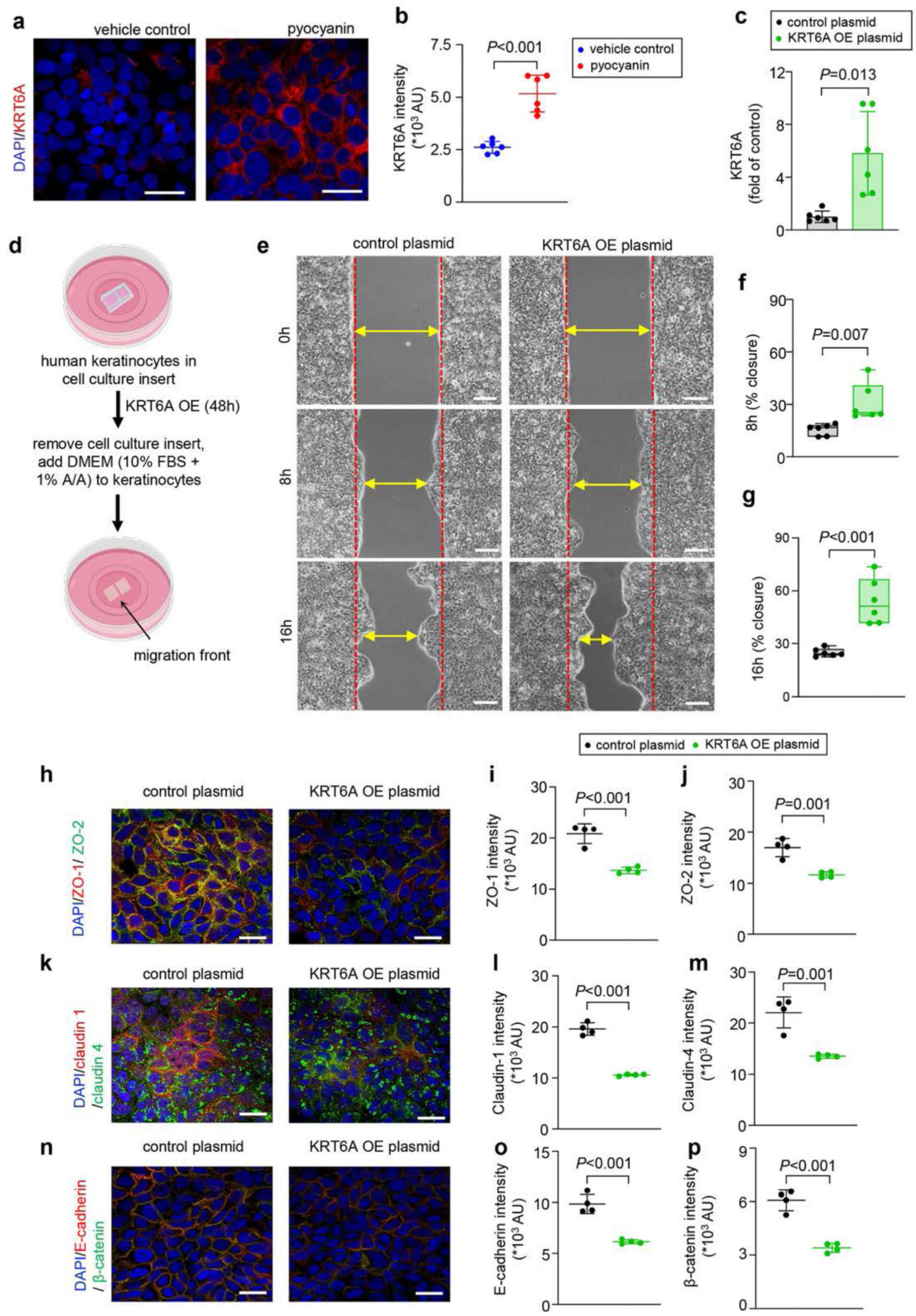

Figure 5. Pyocyanin induced KRT6A for accelerated keratinocyte migration that compromised apical junctional proteins.

(**a-b**) KRT6A expression (**a**) and quantification (**b**) in response to PYO exposure. Scale, 10 µm; n=6. (**c**) KRT6A levels after KRT6A overexpression (48 h) as detected by ELISA; n=6 (**d**) Schematic experimental design (**e**) and keratinocyte migration at 0, 8 and 16 h following 48h KRT6A over-expression, scale, 200 µm. (**f**) Closure (%) in 8 h. (**g**) Closure (%) in 16h; n=6. (**h-p**) Abundance of apical junctional proteins in response to PYO were measured using immunocytochemistry followed by quantitation; n=4 (mean ± SD). KRT6A: Keratin 6A;

OE: over-expression; ZO-1: zonula occludens 1; ZO-2: zonula occludens 2; Scale, 10 μm. All data expressed as mean ± S.D. and were analyzed using Student's t test.

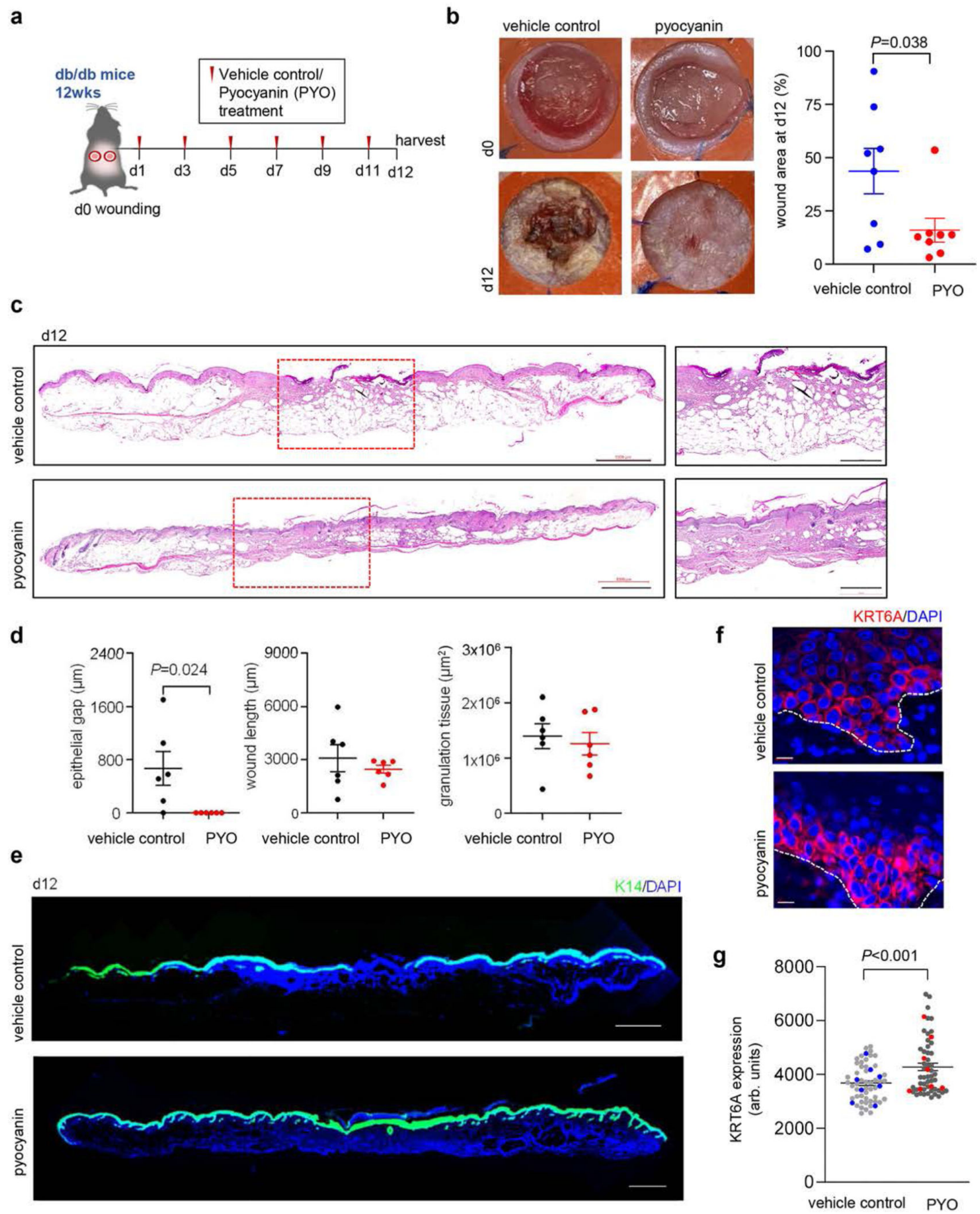

Figure 6. Topical Pyocyanin application accelerated reepithelialization in diabetic mice.

(**a**) Schematic experimental design. (**b**) Digital photographs and quantification of excisional wound. Scale, 2 mm. (**c**) H&E staining of wounds. Scale, 1mm. Inset showing wound-bed. Scale, 0.5mm. (**d**) Morphometric analysis; n=6. (**e**) Keratin 14 immunofluorescence images with DAPI counterstaining. Scale, 500 µm (**f-g**) KRT6A immunofluorescence staining with DAPI counterstaining (**f**) and quantification (**g**). Scale,10µm. Each dot corresponds to one quantified ROI, except the blue and red dots, which correspond to the mean of each mouse. At least 5 ROI per mouse. (n = 8) Data in B and D were analyzed by Student's t test and in g was analyzed by two-way ANOVA to account for the variability within the ROI and across the group.